N95-14456

BENDING EFFECTS OF UNSYMMETRIC ADHESIVELY BONDED COMPOSITE REPAIRS ON CRACKED ALUMINUM PANELS

Cory Arendt and C.T. Sun
School of Aeronautics and Astronautics
Purdue University
West Lafayette, IN 47907

SUMMARY

The bending effects of unsymmetrically bonded composite repairs on cracked aluminum panels were quantified using a plate linear finite element model. Stress intensity factors and strain energy release rates were obtained from the model using the modified crack closure method. The bending effects were quantified by running the model twice, once with out-of-plane displacement suppressed and another time without these restrictions. Several configurations were examined. The effect of the thickness and strength of the adhesive and repair layer was determined, crack growth stability was identified, and the effect of a debond was considered. The maximum stress intensity factor was also analyzed. Previous work by other authors was found to underpredict the bending effect.

INTRODUCTION

In the late 1970's the Royal Australian Air Force developed a method to arrest fatigue and corrosion crack growth in their aircraft through the application of adhesively bonded composite repairs. Since then, many researchers have addressed the problem from a theoretical standpoint and developed methods to predict the stress intensity factors at the crack tip for various patch configurations. Tierang Liu and Weixun Fan[3], Poole, Brown, and Young[4], and Young, Cartwright, and Rooke[5] have used either finite element, boundary element, or numerical analysis to calculate the stress intensity factors using 2-D models without considering out-of-plane deformation. In the actual application of a repair to the fuselage or wing section of an aircraft, the repair can only be applied to the outer accessible side. Hence, the repair is applied unsymmetrically with respect to the loading axis. With the application of the unsymmetric repair, the neutral axis of loading has shifted outward from the cracked plate, resulting in localized bending of the repaired region. This localized bending leads to further opening of the crack face farthest from the repair. Because of this out-of-plane deformation, the 2-D solutions are no longer valid unless a bending correction factor is included. Jones, Callinan, and Aggrawal[6] developed their own finite element code based upon the shear stress profile of a symmetrically patched configuration. In their development, they acknowledged the bending effect and adjusted the shape functions to account for the single sided patched configurations. However, they made no attempt to actually account for the difference in stress intensity factors for unsymmetric and symmetric repair configurations.

Ratwani[1] was the first to address the bending effect from a strength of materials approach. He utilized the finite element code NASTRAN to calculate the stress intensity factor with a specialized crack

tip element. In the model, the plate and repair were composed of 2-D plate elements while the adhesive layer was composed of prismatic shear elements. As a result, the adhesive layer was not an elastic continuum, but rather a layer which only transferred shear loads. An elliptical debond between the cracked plate and the adhesive layer was introduced into the model. The repair and plate were considered to be of the same material and size. The results, which did not account for out-of-plane deformation, were then adjusted to correct for the bending effect. The difference between the load carried by the cracked layer and the load carried by the repaired layer resulted in a global moment. This moment was then applied to the entire structure and the increased stress due to bending was included in the stress intensity factor. Experiments were performed and the bending effect was found to have an average of 27% increase in the normalized stress intensity factor.

Rose[2] used a theoretical basis to develop a solution for a finite length patch configuration. In this he used shear lag analysis to calculate an effective adhesive load transfer length. The adhesive layer was removed and the crack extended an amount over which the shear load could not transfer. To simplify the theory, the repair was assumed to be of infinite length. From slender beam deflection theory, and equilibrium, Rose developed expressions for the deflection of the repair and unrepaired section in the out-of-plane direction. These deflections were transformed into moment expressions for the patched and unrepaired region. A total reaction moment at the crack location was calculated. By integrating the reaction moment over the thickness of the repair, the strain energy caused by bending was calculated. The total strain energy release rate was then obtained by superimposing the energy needed to close the crack in the in-plane direction with the strain energy needed to bend the structure back to its original position.

Ratwani and Rose's solution cannot be compared because they are derived for entirely different patch configurations. It is the object of this study to use a plate finite element model to accurately predict the 3-D bending effects. Comparisons between the results of the present model and both Ratwani's and Rose's work were made.

The effects of a debond, variations in adhesive and repair properties were investigated. Crack stability along with extrapolation of the maximum stress intensity factor from the average value finite element results were discussed.

PRESENT MODEL

Using the commercial finite element code ANSYS, a 2-D bonded repair model was created. The aluminum plate and repair were modeled using 4-noded shell elements with five degrees of freedom (u_x, u_y, u_z, θ_x, and θ_y) at each node. The adhesive layer was represented by shear springs in the x and y directions. Attempts were made to model the adhesive layer as an elastic continuum using 3-D, 8-noded brick elements. However, due to the adhesive layer's relatively small thickness, severe numerical errors were encountered. This occurred because the aspect ratios of these elements far from the crack tip grew to unreasonably high proportions. The plate and repair were modeled using rectangular elements. The nodes of each layer coincided identically in space with respect to the x and y directions as shown in Figure1. The spring elements used to model the adhesive layer were one dimensional. Only the two

shear springs at each node were included in the model. The spring constants were developed on the assumption that the adhesive layer would transfer only shear loads. The relation between the shear nodal forces and in-plane nodal displacements is given by:

$$\frac{F}{A} = \mu \frac{(u_{Upper} - u_{Lower})}{t_{Adhesive}} \tag{1}$$

where μ is the shear modulus of the adhesive and A is the area represented by the shear spring. These shear spring constants in the x and y directions were found to be a function of the element's area and were distributed evenly among the four nodes.

$$k_x, k_y = \frac{\mu A}{4 t_{Adhesive}} \tag{2}$$

Since each element consists of a different area, the spring constants varied from node to node.

In order to connect the outer layers to the inner spring elements, constraint equations were imposed. These constraint equations provided continuity along the adhesive/plate interface and adhesive/repair interface. The equations related the rotational deformation and in-plane displacement of the shell elements to the displacement of the spring elements (see Figure 1). Four nodes existed in the z direction for each x-y coordinate. The outer two nodes were part of the plate and repair layers, while the 2 springs were connected to the inner two nodes. The constraint equations were implemented in the x, y, and z directions. For the x-direction:

$$u_{x2} = u_{x1} - \frac{t_{Repair}}{2}\theta_{y\ Repair} \qquad u_{x3} = u_{x4} + \frac{t_{Plate}}{2}\theta_{y\ Plate} \tag{3}$$

y-direction:

$$u_{y2} = u_{y1} + \frac{t_{Repair}}{2}\theta_{x\ Repair} \qquad u_{y3} = u_{y4} - \frac{t_{Plate}}{2}\theta_{x\ Plate} \tag{4}$$

z-direction:

$$u_{z2} = u_{z1} \qquad u_{z3} = u_{z4} \tag{5}$$

STRAIN ENERGY RELEASE RATE CALCULATIONS

The modified crack closure method [7] was used to calculate the strain energy release rate. The crack closure method allows for the calculation of the strain energy release rate by calculating the strain energy at a single crack length. The crack size was increased a finite amount when the model was run a second time. The difference in strain energy between these two cases divided by the increase in crack length produced the desired strain energy release rate. Since this method was time consuming, the modified crack closure method was developed. It assumed that the strain energy release rate could be obtained in one run of the model if the widths of the two crack tip elements were identical and the ratio of the width of the crack tip element to the length of the crack, itself, was less than 10%. In this model crack opening was considered to be Mode I. Without the out-of-plane bending effect, the crack growth was entirely Mode I. However, when out-of-plane deformation did occur, the crack opening increased on the side furthest from the repair. This caused the crack face to rotate, allowing the crack to open even more. Thus, for out-of-plane deformation, two strain energy release rates had to be calculated: One to

close the crack tip in terms of the displacement and a second to rotate the crack face back to its original position.

The strain energy release rate due to translational displacement was calculated by:

$$G_{Iu} = \frac{1}{2\Delta a}\left\{F_{yA}(u_{yB} - u_{yC})\right\} \tag{6}$$

The strain energy release rate due to rotation was calculated by:

$$G_{I\theta} = \frac{1}{2\Delta a}\left\{M_{xA}(\theta_{xB} - \theta_{xC})\right\} \tag{7}$$

The total strain energy release rate is the sum of these two calculations. By calculating the total strain energy release rate for different mesh configurations, convergence could be examined. Figures 2 and 3 demonstrated mesh convergence with respect to element size along the x and y directions. The converged mesh properties chosen for all models were $\Delta a / a = .075$ and $\Delta L = .005$.

MODEL VERIFICATION

In an effort to verify the constraint equations and spring constants, the model was altered to compare it to the results generated by Young [8]. In [8], center cracked plates were subjected to uniform bending moments.A single plate finite element model was used to calculate the normalized strain energy release rate. In the present study, a similar finite element mesh was created using ANSYS. Verification of the constraints came about by removing the adhesive layer in the spring model and comparing the results of this two plate model to a single plate. The adhesive layer in the spring model was removed because the shear springs were not designed to undertake large scale bending deformation. The two plate configuration was tied together solely by constraint equations and gave identical results to the single plate solution. The difference between Young's results [8] and the single and double plate configurations differed by less than .5% (see Figure 4).

The spring constants were verified by checking if the spring model would converge to the two plate configuration. Figure 5 demonstrates how the spring model successfully converged to the two plate solution.

COMPARISONS

Comparison to Ratwani's [1] finite element results was performed. Ratwani experimented with several different repair configurations, but only one model considered the bending effect. The center cracked aluminum plate under axial tension was repaired with an aluminum patch. The repair was the same size as the plate. Utilizing symmetry, only a quadrant of the plate was modeled. An elliptical debond between the plate and the adhesive layer existed in order to facilitate the use of the specialized crack tip element.

The present model was built to the same specifications as in Ratwani's work. The model was then run twice for each crack length, once with the following boundary conditions for having no out-of-plane deformation :

$$\begin{aligned} &@x = 0 && u_x = 0 && \theta_y = 0 \\ &@y = 0,\ x > a,\ z = \frac{t_{Plate}}{2} && u_y = 0 && \theta_x = 0 \\ &@y = 0,\ z \neq \frac{t_{Plate}}{2} && u_y = 0 && \theta_x = 0 \\ &@\text{all nodes} && u_z = 0 \end{aligned} \tag{8}$$

In the second run the constraints in the z direction at all the nodes except for the one at the origin of the plate were released. An elliptical debond with semi-minor to semi-major axis ratio of b/a = .10 was included (see Figure 1). The semi-major axis coincided with the crack length a. The debond was simulated by removing the constraints between the plate and adhesive layer. The results are presented in Figure 6.

With no consideration for bending, the present model underpredicted Ratwani's results, that also did not include bending, by an average of 6% over a set of five crack lengths. This discrepancy could be accounted for by the difference in convergence directions. Ratwani's use of the specialized crack tip element resulted in convergence from above the actual value. The modified crack closure method, on the other hand, reached a converged solution from below the actual value. Once Ratwani's results were corrected for bending and compared to the present model, which was allowed to displace in the out-of-plane direction, the present model overpredicted Ratwani's results by more than 11.5%. Ratwani's results also showed that the bending effect could increase the normalized stress intensity factor by over 27%, while the present model demonstrated a 52% increase. Thus on average, Ratwani underpredicted the present model's bending effect by about 25%.

Rose [2] developed an analytical expression to calculate the value of the strain energy release rate for a patched configuration undergoing out-of-plane deformation. Rose developed his solution based upon a patch of a finite length instead of a full length patch. His expression was a function of all the thicknesses and material properties involved. In order to make a valid comparison of Rose's expression, the present model was run for several different cases to find possible regimes where the theory broke down. Figure 7 demonstrated how the two models compared when examining the trends in the adhesive layer. Both accurately predicted the increasing trend in total strain energy release rate as the adhesive thickness increased and adhesive shear modulus decreased. The average difference between all three cases resulted in the present model overpredicting the total strain energy release rate by 176%. A similar test was run for the variation in repair properties (see Figures 8a and 8b). In this case, the present model results showed a definite decreasing trend as the repair stiffness increased. Rose's model, in this case, did not provide a consistent trend indicating that his model was not able to predict expected values in all regimes.

CRACK STABILITY

Rose's model was based upon a prediction that the strain energy release rate would reach a limiting value as the crack grew. Because of this limiting value, a characteristic crack length could be calculated. This limitation was based upon the maximum displacement allowed by the cracked surface derived in the shear lag analysis. This derivation was performed for the case when bending was suppressed. However, when calculating the increase in strain energy release rate due to bending, this assumption remained true. Therefore, Rose assumed a characteristic crack length would also exist when bending was introduced. When the models that accounted for bending were run for various crack lengths, the strain energy release rate failed to reach a limit (see Figure 9). The values for the spring model increased, while Rose's model was not affected by the variation in crack length. In the case where bending was suppressed for the present model, it was demonstrated that the strain energy release rate remained constant. Thus, it was proven that Rose's application of the shear lag analysis was correct in the case where bending was suppressed, but not applicable in the case when bending did exist.

An increase in the strain energy release rate indicated crack growth instability. This result was viewed with skepticism. In order to determine the validity of this finding, the patch was removed and the model was re-run. Figure 10 demonstrated the increasing rate of instability of the single plate. With this plot, the boron repair configuration with out-of-plane bending was also found to be relatively stable on this new scale. Therefore, it could be concluded that unsymmetric patch configurations may possess crack growth instability. However, comparison of this instability for the unsymmetric patch configuration to the instability for a single plate was found to be relatively minor.

DEBOND EFFECTS

The effects of the debond size were next considered. Following Ratwani's experimental finding [1] that the elliptical debond begins at the crack tip, different elliptical debond sizes were considered. Having fixed a semi-major axis of the ellipse as the crack length a, the semi-minor axis b was varied. It can be seen in Figure 11 that a change in the debond's elliptical shape produced a negligible increase in the strain energy release rate for a certain crack length. When the effect of the inclusion of a debond was considered, the effect was much more pronounced. Figure 12 depicted the difference in a boron repair model with and without a debond and with and without bending. When bending was not considered, the inclusion of a debond increased the strain energy release rate by an average of 200%. In a similar manner, the debond for the case where bending was included increased the strain energy release rate by 88%.

MAXIMUM STRESS INTENSITY FACTOR

The total strain energy release rate calculated from the finite element model was based upon the displacement and rotation at the mid-plane of the crack plate. When bending occurred, the crack opening

increased on the side furthest from the repair. This caused the crack face to rotate, allowing the crack to open further. The amount of energy gone into opening the crack face in the in-plane direction was 97%, while the remaining 3% went into rotating the crack face. From the finite element results, the rotation seen by the mid-plane node was less than a fraction of a degree. From these results, it was concluded that the rotation of the crack face was minor. Therefore, the variation in the strain energy release rate through the thickness of the plate varied a negligible amount. This also indicated that the bending effect does not deform the local crack tip region in the out-of-plane direction. Instead, the bending effect is a global phenomenon. Thus, plane stress relationships held near the crack tip. From plane stress fracture mechanics, the stress intensity factor was obtained from:

$$K = \sqrt{\frac{G_{Total} E_{Plate}}{t_{Plate}}} \tag{9}$$

The variation in the stress intensity factor through the thickness is negligible.

When the normalized stress intensity factor was plotted against the crack growth of a boron repair configuration, the values decreased (see Figure 13). In terms of the normalized stress intensity factor, the effect of bending on a model without a debond was an increase of 520%, while a model with a debond experienced a 400% increase.

CONCLUSIONS

This paper has presented a successful development of a plate finite element model which can be used to predict the bending effects of a bonded composite repair configuration. Constraint equations and shear springs were incorporated into the model to accurately represent the out-of-plane deformation that occurs in unsymmetric patch configurations. The modified crack closure method produced results within 6% of Ratwani's in-plane deformation results obtained through the use of special crack tip elements.

The following conclusions were obtained:

- Ratwani's model underpredicted the present models results by 25% in terms of the normalized stress intensity factor.
- Rose's analytical solution underpredicted the total strain energy release rate for several adhesive thicknesses by an average of 176%.
- For the repair variation analysis, Rose's theory produced an inconsistent trend.
- The total strain energy release rate increased as the adhesive thickness increased and shear modulus decreased.
- The total strain energy release rate decreased as the stiffness of the repair increased.
- Crack growth instability occurred for the unsymmetric repair. However, it was relatively stable as compared to the instability of an unrepaired crack.
- A debond increased the total strain energy release rate by 200% when no bending occurred, and 88% when bending was present.
- The variation of stress intensity factor over the thickness of the cracked plate is negligible.

REFERENCES

1. Ratwani, M.M.: Characterization of Fatigue Crack Growth in Bonded Structures. AFFDL-TR-77-31 Volume II, June 1977, pp.55-64.

2. Baker, A.A.; and Jones, R.: Bonded Repair of Aircraft Structures. Martinus Nijhoff Publishers, 1988, pp. 77-98.

3. Liu, Tierang; and Fan, Weixun.: Analysis for an Adhesively Bonded Finite Strip Repair to a Cracked Plate. *Engineering Fracture Mechanics*. vol.47, no. 5, pp. 629-637.

4. Poole, P.; Brown, K.; and Young, A.: Adhesively Bonded Composite Patch Repair of Thick Sections. *Fatigue and Fracture Mechanics*. 1988.

5. Young,A.; Cartwright,D.J.; and Rooke, D.P.: The Boundary Element Method for Analysing Repair Patches on Cracked Finite Sheets. *The Aeronautical Journal of the Royal Aeronautical Society,* December 1988.

6. Jones,R.; Callinan,R.J.; and Aggrawal,K.C.: *Analysis of Bonded Repairs to Damaged Fibre Composite Structures. Engineering Fracture Mechanics.* vol.17, no.1, pp.37-46.

7. Rybicki, E.F.; Kanninen, E.F.: A Finite Element Calculation of Stress Intensity Factors by a Modified Crack Closure Integral, *Engineering Fracture Mechanics*, 1977 vol.9 pp.931-938.

8. Young, Min Jho: Analysis of Cracked Plates Subjected to Out-of-Plane Loadings, Ph. D. Thesis, Purdue University, 1991.

ACKNOWLEDGMENT

This work was supported by the Air Force Office of Scientific Research through a University Research Initiative Grant No. NTP1397 to Purdue University.

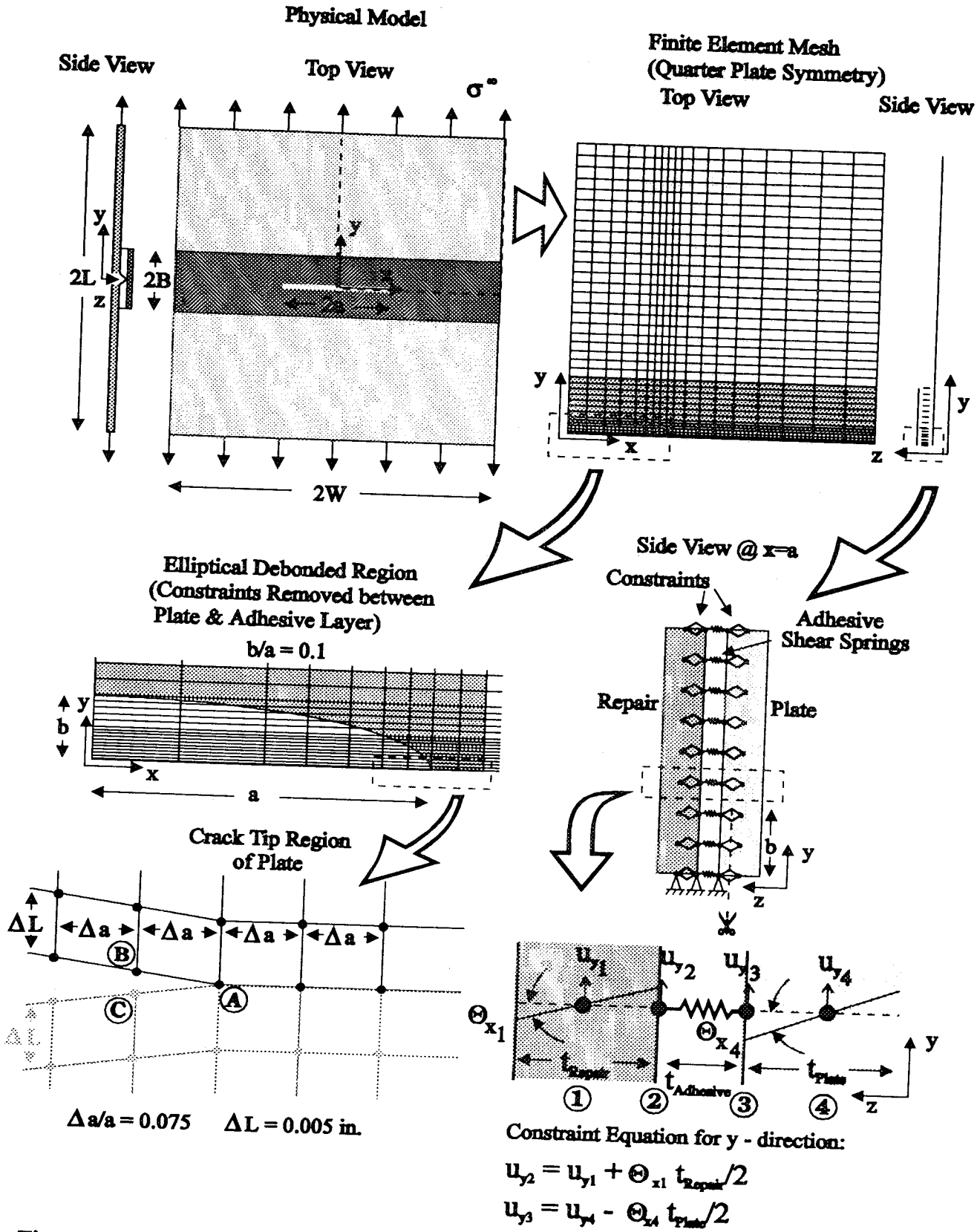

Figure 1. Finite Element Model for the Adhesively Bonded Repair of Cracked Aluminum Plates.

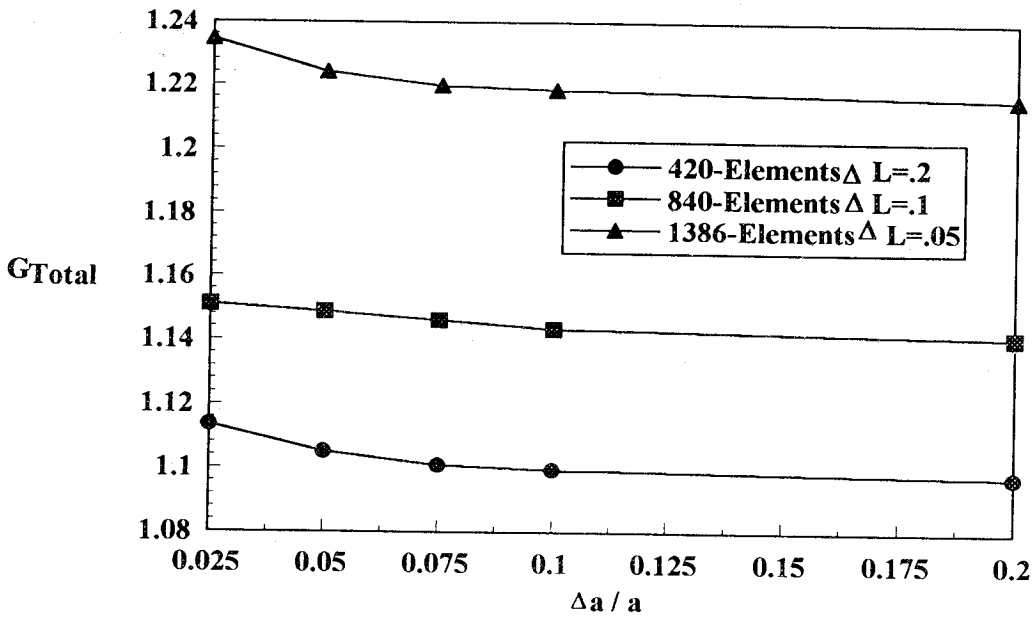

Figure 2 **Mesh Convergence with respect to element size along x-axis.**
$E_{Repair} = 10.3 \times 10^6$ psi. $E_{Plate} = 10.3 \times 10^6$ psi. $\mu_{Adhesive} = 3.872 \times 10^6$ *psi.*
t_{Repair} =.1181 in. t_{Plate} =.1181 in. $t_{Adhesive}$ =.009 in. σ^{∞} = 16935 psi. ν=.33
L=10 in. W=10in. B=2.0 in. a=3.0 in.

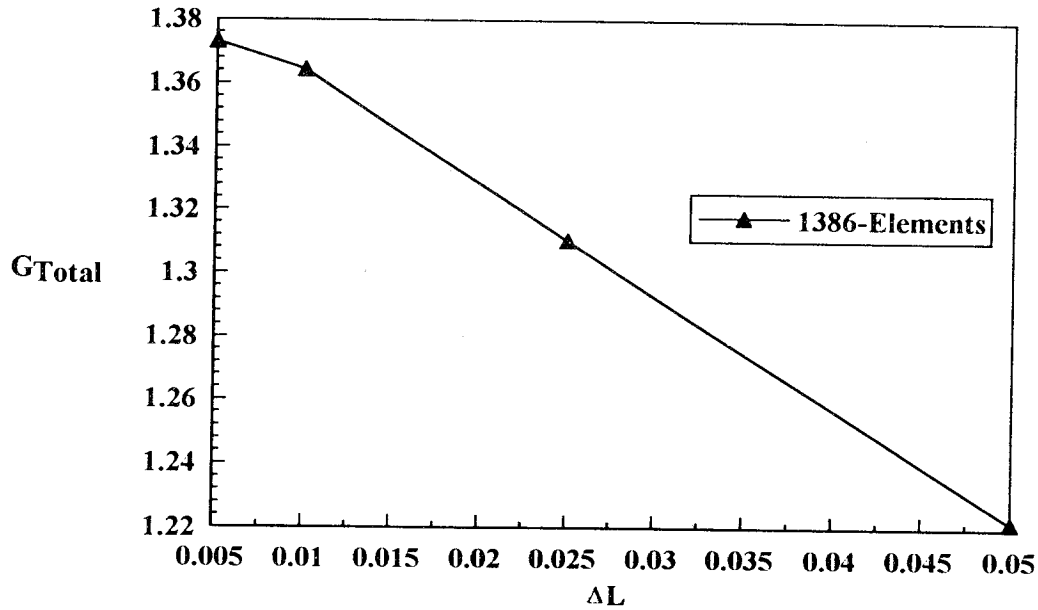

Figure 3 **Mesh convergence with respect to element size along y-axis.**
Δa / a =.075.

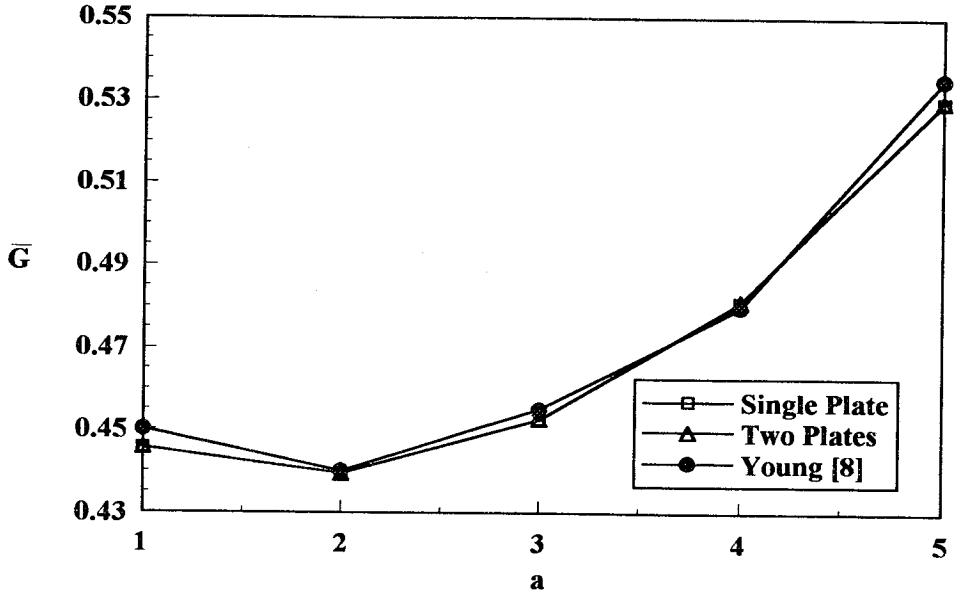

Figure 4 **Comparison of normalized $\overline{G} = G_{Total} Eh^3 / 12M^2 a\pi$ for a center cracked plate subjected to uniform bending moment.** $\Delta a / a = .10$ $E = 3.0 \times 10^6$ psi. h=.3 in. M=1500 in.lb. L=10.0 in. W= 10.0 in.

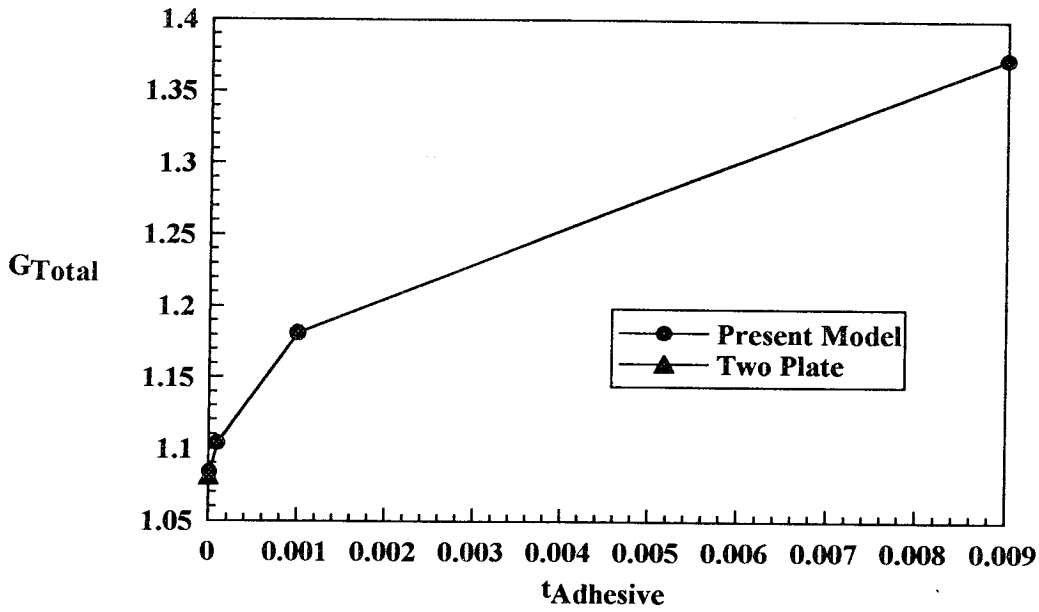

Figure 5 **Convergence of Present Model to Two Plate Solution.**
$E_{Repair} = 10.3 \times 10^6$ psi. $E_{Plate} = 10.3 \times 10^6$ psi. $\mu_{Adhesive} = 3.872 \times 10^6$ *psi.*
$t_{Repair} = .1181$ in. $t_{Plate} = .1181$ in. $\sigma^{\infty} = 16935$ psi. $\nu = .33$
L=10 in. W=10in. B=2.0 in. a=3.0 in.

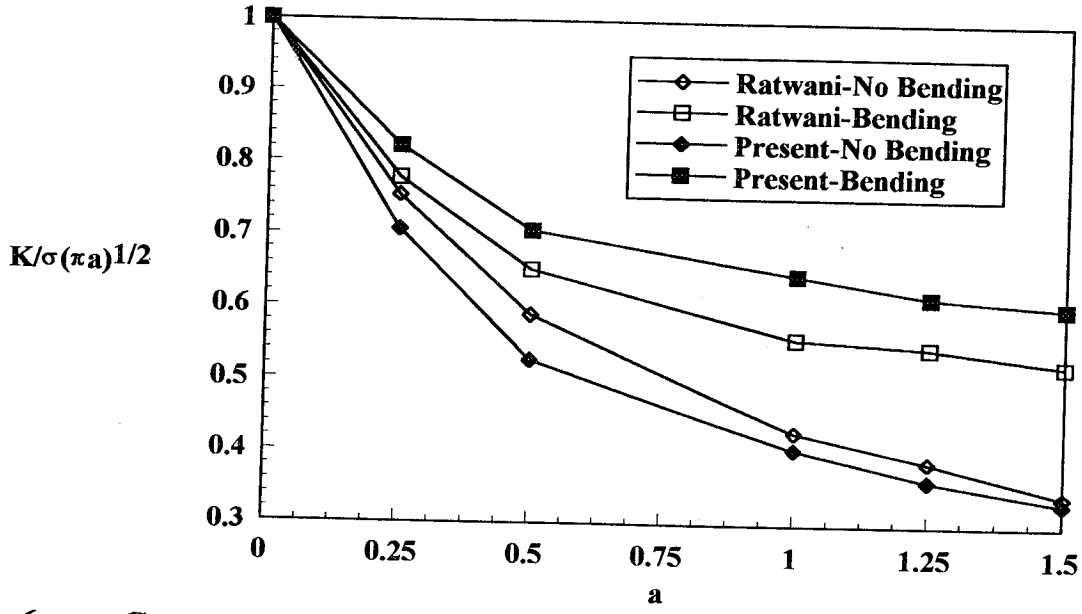

Figure 6 **Comparison to Ratwani's Bending Correction Factor.**
$E_{Repair} = 10.3 \times 10^6$ psi. $E_{Plate} = 10.3 \times 10^6$ psi. $\mu_{Adhesive} = 6.0 \times 10^4$ *psi.*
t_{Repair} =.063 in. t_{Plate} =.063 in. $t_{Adhesive}$ =.008 in. σ^{∞} = 16935 psi. ν=.33
L=6 in. W=3 in. B=6 in. Elliptical Debond b/a=.10

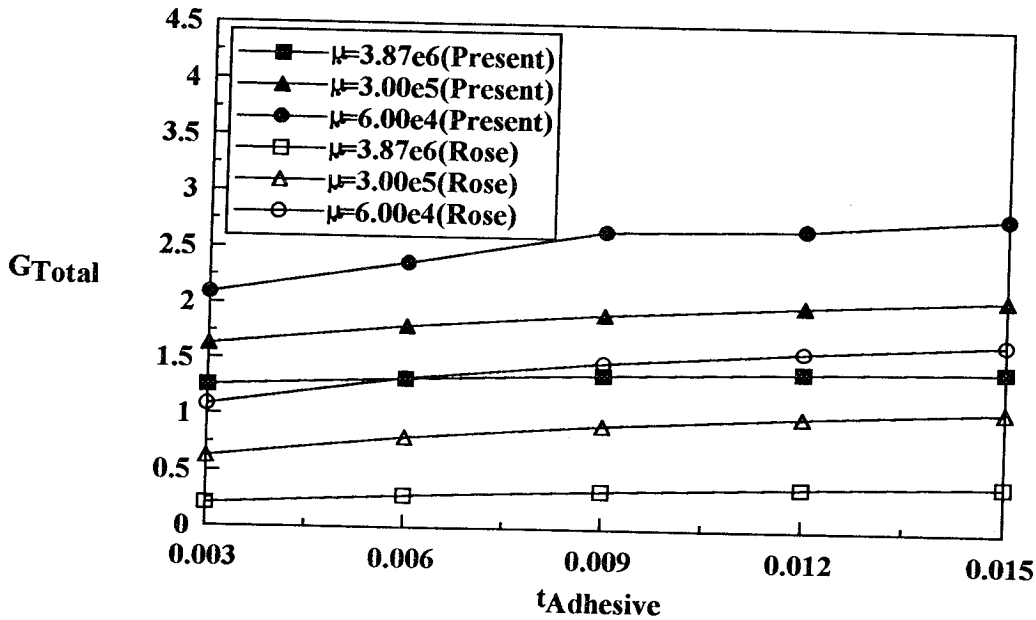

Figure 7 **Comparison to Rose's Analytical Solution for variations in adhesive thickness and adhesive shear modulus.**
$E_{Repair} = 10.3 \times 10^6$ psi. $E_{Plate} = 10.3 \times 10^6$ psi.
t_{Repair} =.1181 in. t_{Plate} =.1181 in. σ^{∞} = 16935 psi. ν=.33
L=10 in. W=10in. B=2.0 in. a=3.0 in.

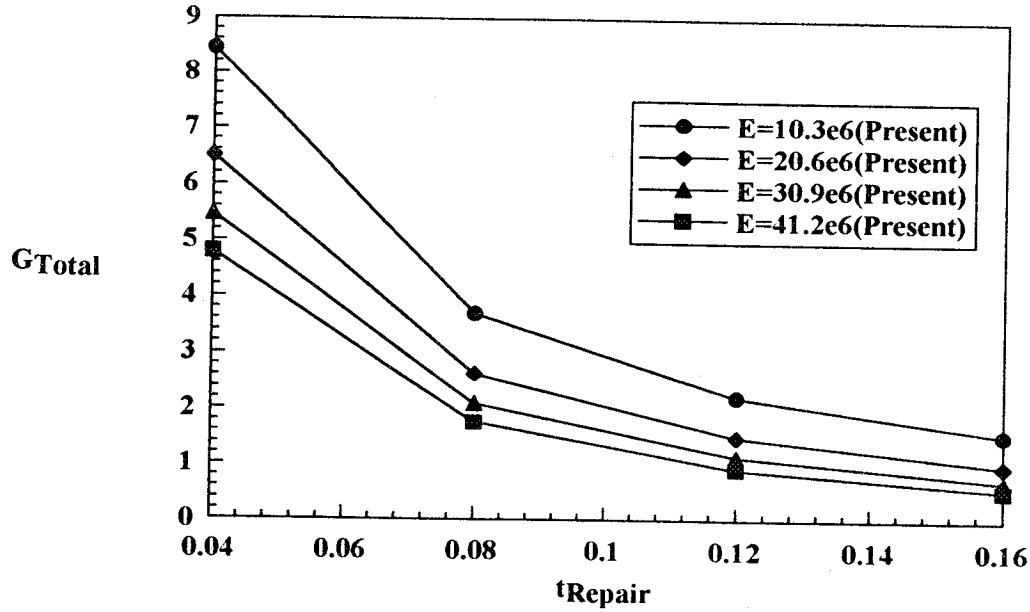

Figure 8a **Present solution for variations in repair thickness and repair modulus.**
$E_{Plate} = 10.3 \times 10^6$ psi. $\mu_{Adhesive} = 1.015 \times 10^5$ *psi*
t_{Plate} =.1181 in. $t_{Adhesive}$ =.008 in. σ^{∞} = 16935 psi. ν=.33
L=10 in. W=10in. B=2.0 in. a=3.0 in.

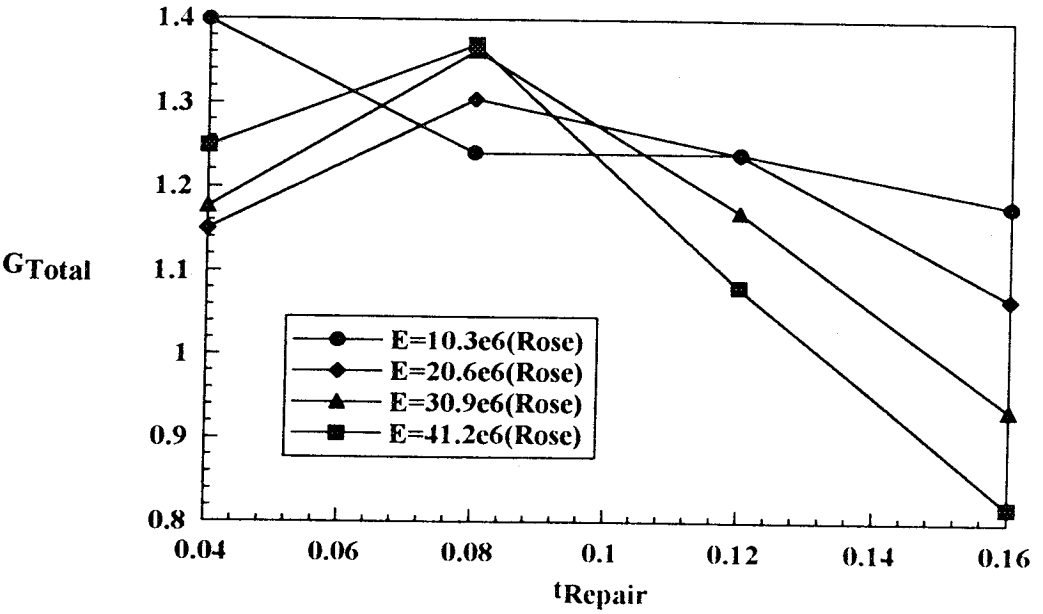

Figure 8b **Rose's analytical solution for variations in repair thickness and repair modulus.**

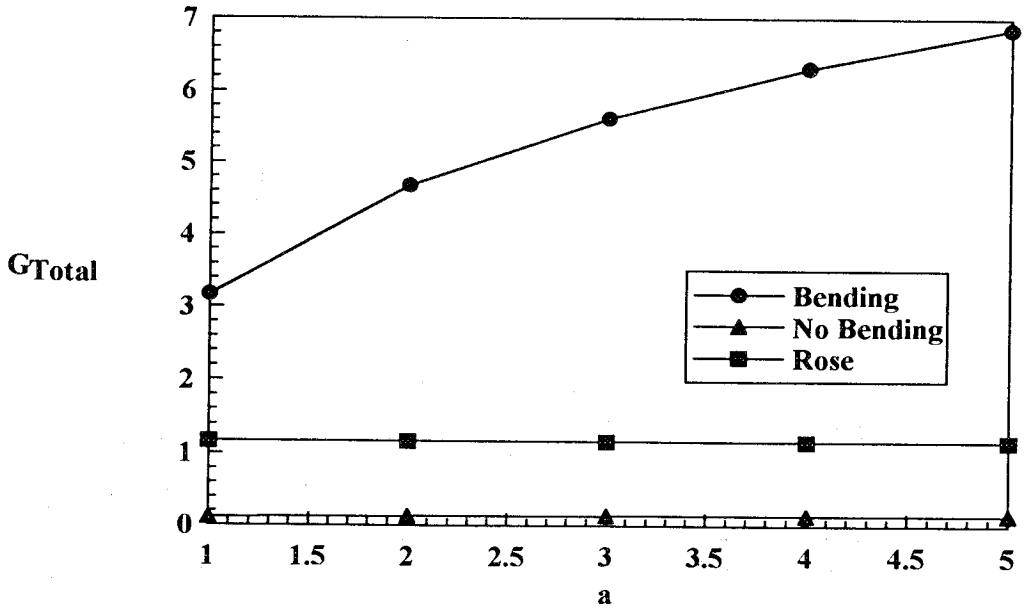

Figure 9 **Crack Trend for Boron Repair Scheme.**

$E_{Repair} = 29.0 \times 10^6$ psi. $E_{Plate} = 10.3 \times 10^6$ psi. $\mu_{Adhesive} = 1.015 \times 10^5$ *psi*

t_{Repair} =.04 in. t_{Plate} =.1181 in. $t_{Adhesive}$ =.008 in. σ^{∞} = 16935 psi. ν=.33

L=10 in. W=10in. B=2.0 in.

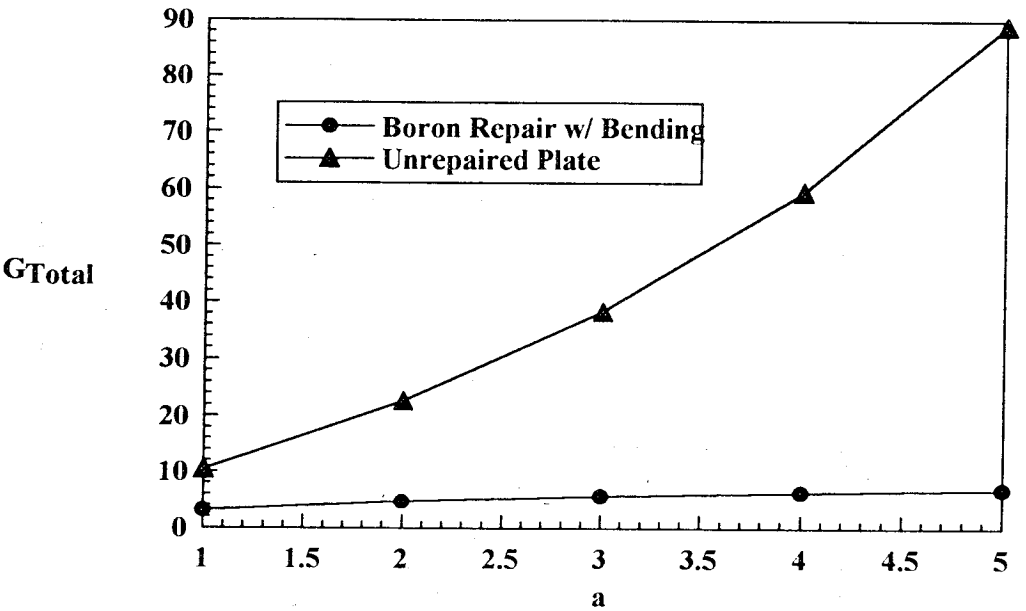

Figure 10 **Crack Stability for various crack lengths.**

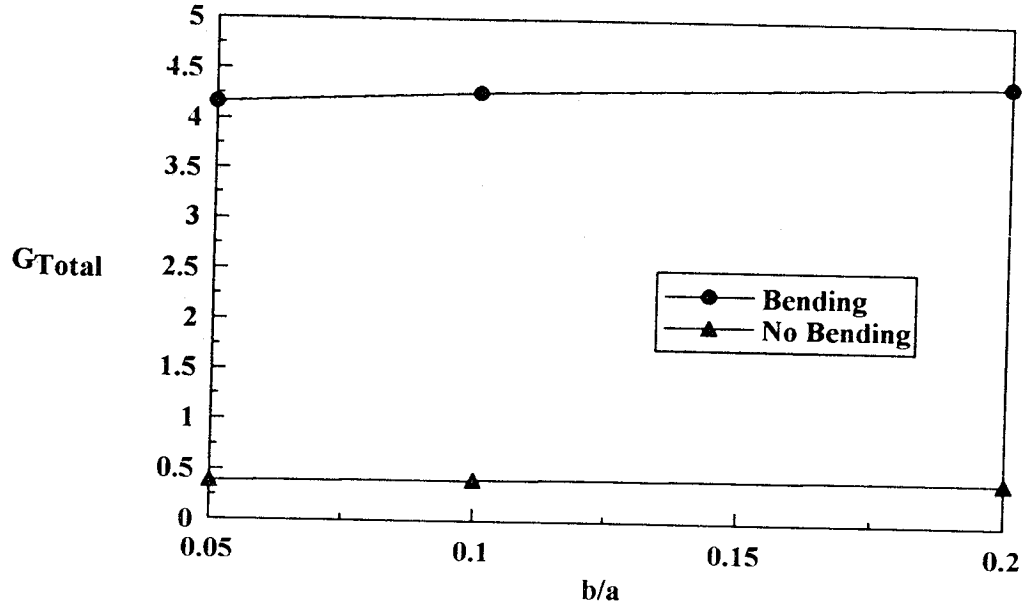

Figure 11 **Comparison of elliptical debonds of various aspect ratios.**
$E_{Repair} = 29.0 \times 10^6$ psi. $E_{Plate} = 10.3 \times 10^6$ psi. $\mu_{Adhesive} = 1.015 \times 10^5$ *psi*
t_{Repair} =.04 in. t_{Plate} =.1181 in. $t_{Adhesive}$ =.008 in. σ^{∞} = 16935 psi. ν=.33
L=10 in. W=10in. B=2.0 in. a=1.0 in.

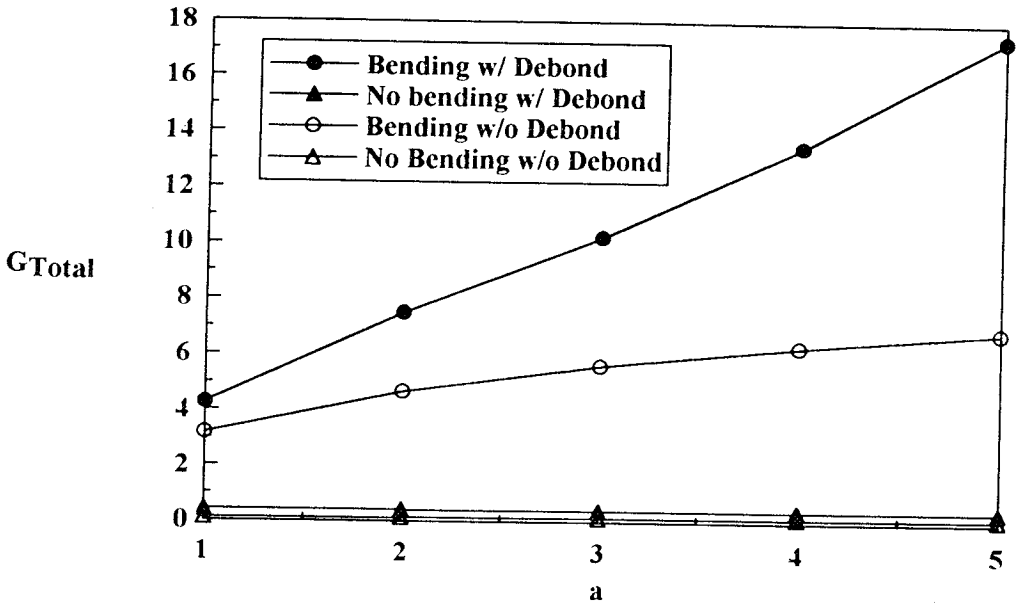

Figure 12 **Crack Growth for boron repair scheme with elliptical debond.** b/a=.10
$E_{Repair} = 29.0 \times 10^6$ psi. $E_{Plate} = 10.3 \times 10^6$ psi. $\mu_{Adhesive} = 1.015 \times 10^5$ *psi*
t_{Repair} =.04 in. t_{Plate} =.1181 in. $t_{Adhesive}$ =.008 in. σ^{∞} = 16935 psi. ν=.33
L=10 in. W=10in. B=2.0 in.

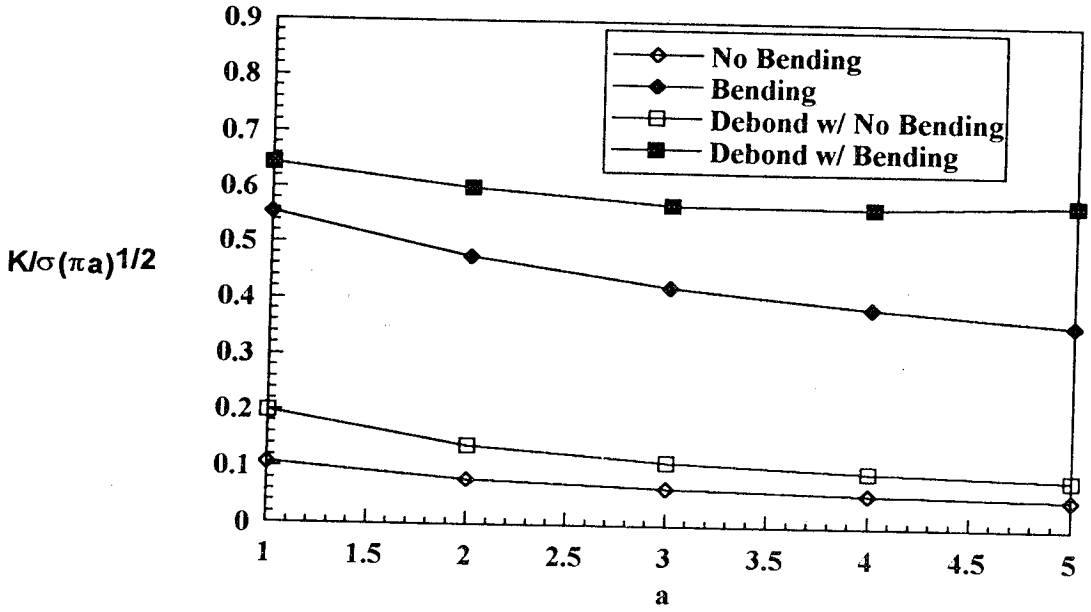

Figure 13 **Crack growth trend for a boron repair scheme**. Debond b/a= .10 $E_{Repair} = 29.0 \times 10^6$ psi. $E_{Plate} = 10.3 \times 10^6$ psi. $\mu_{Adhesive} = 1.015 \times 10^5$ *psi* t_{Repair} =.04 in. t_{Plate} =.1181 in. $t_{Adhesive}$ =.008 in. σ^{∞} = 16935 psi. ν=.33 L=10 in. W=10in. B=2.0 in.